Eur. Phys. J. D **18**, 87–92 (2002)
DOI: 10.1140/e10053-002-0011-x

THE EUROPEAN PHYSICAL JOURNAL D
EDP Sciences

Electron impact excitation of krypton clusters

C. Malone, W. Kedzierski, and J.W. McConkey[a]

Department of Physics, University of Windsor, Windsor, Ontario, N9B 3P4, Canada

Received 29 August 2001 and Received in final form 31 October 2001

Abstract. A detailed study has been made of the fragmentation of neutral krypton clusters following electron impact. The vacuum ultraviolet fluorescence and metastable fragments were monitored using a time-of-flight technique. Fragment kinetic energy distributions were obtained, showing that the fastest fragments were ejected with energies near 1 eV. Slower fragments with a peak kinetic energy near 0.5 eV were observed to dominate the fragmentation at higher incident electron energies. At least six processes were observed to contribute to cluster break-up with some of these involving exciton production. At least three further processes involved vacuum ultraviolet photon production.

PACS. 34.80.Gs Molecular excitation and ionization by electron impact – 36.40.-c Atomic and molecular clusters

1 Introduction

Krypton is a valuable continuum light source in the vacuum ultraviolet (VUV) [1,2]. Pulsed lasing in the VUV has also been observed *via* Kr excimers [3] and various non-linear techniques [4–6]. Situations involving relatively high pressure can generate clusters that have even been shown to increase harmonic radiation yields when using xenon [7]. In addition, there has been considerable interest in the excitation of Kr clusters, in the various mechanisms that can occur, in the different possible decay channels, and in how the size of the cluster influences the outcome. Much of the experimental work has involved synchrotron radiation [8–17]. Kamke *et al.* [8] and Krauss *et al.* [9] investigated rare gas clusters (RGCs) using threshold-photo-electron-photoion-coincidence (TPEPICO) time-of-flight (TOF) techniques to detect ions correlated with zero-kinetic-energy-electron emission. Ganteför *et al.* [10] also used a TOF technique to investigate photoionization thresholds of RGCs. Photoionization of RGCs was also investigated by Thissen *et al.* [11] in the inner valence shell region. Recently, site-specific inner shell excitation in Kr clusters was studied using synchrotron radiation [12]. In many cases in the study of neutral Kr clusters the total unresolved fluorescence was observed as a function of incident photon wavelength, so-called fluorescence excitation spectroscopy [13,14]. In some cases [14] the fluorescence was wavelength analyzed and in others [15] the temporal behaviour of the fluorescence was investigated.

Electron impact excitation (1 keV) has been used by Verkhovtseva *et al.* [18] to investigate rare gas clusters. In these studies, Kr cluster fluorescence in the VUV was wavelength-resolved. The VUV spectrum from reference [18] shows several features, in addition to the atomic resonance lines, resulting from cluster effects. Bondarenko *et al.* [19] later re-examined the VUV spectrum of the rare gas clusters by electron impact (same conditions) as a function of mean cluster size. For Kr clusters, an additional feature peaked at 159 nm was observed with larger mean cluster sizes. The spectral peak at 159 nm was attributed to radiative decay of Kr excimers formed in ionic Kr clusters. Karnbach *et al.* [17] observed a broad continuum between 126 and 142 nm for small ($N < 50$) Kr clusters (using synchrotron radiation), which was not identified in references [18,19]. This continuum is attributed to the decay of krypton excimers desorbing from the cluster surface. Interestingly, Gerasimov *et al.* [2] show several data plots with this 126–142 nm continuum, though no distinct identification was made.

The present work involving electron beam excitation of Kr clusters is a continuation of previous argon cluster studies [20,21]. A variety of techniques have been used to probe the electron-cluster interaction, to obtain spectroscopic information on the potential energy curves of the Kr dimer and to obtain significant new information on the cluster dissociation dynamics. The work compliments the wealth of information that is currently available from photon impact studies.

2 Experiment

The experimental details have been previously discussed by our group [20–23], so only a brief outline will be included here. Clusters are produced using a room-temperature piezo-electric pulsed valve, typically

[a] e-mail: mcconk@uwindsor.ca

operating at a stagnation pressure of 3.5 atm, a pulse width of 150 μs, and a repetition rate of 65 Hz. The 0.25 mm conical nozzle is at a distance of 15 mm from a 1 mm diameter skimmer that separates the differentially pumped expansion and collision chambers. Under these conditions an average cluster size in the hundreds was estimated using the procedure in references [24,25]. Alternatively, the valve could be operated under conditions where insignificant clustering, as observed by the time-of-flight (TOF) mass spectrometer in-line with the gas beam, occurred. A pulsed electron beam intersected the gas beam at right angles within the collision chamber.

Photons or metastable fragments from the interaction region were detected as a function of time after the exciting electron pulse using a CsI-coated channel electron multiplier (channeltron) located as illustrated in Figure 1 of reference [20]. The upper wavelength cut-off of the channeltron was determined by the CsI coating and was approximately 180 nm though, from the work of Bondarenko *et al.* [19] and Möller *et al.* [26], insignificant VUV emissions from the clusters at wavelengths longer than 180 nm should be expected. Excitation functions were obtained by ramping the electron energy while collecting the fluorescence photons or metastable fragments. Data specific to a particular time window (fragment velocity range) could be recorded. The electron beam current was simultaneously monitored so that the excitation function intensities could be corrected. This was only important at the lowest electron energies, below about 30 eV. The electron energy was calibrated using the onset for Kr^+ formation at 14.00 eV (88.59 nm) [8–10]. During this calibration, which was made using the mass spectrometer, all parameters were maintained as close as possible to the values used during the excitation function measurements. Hence changes in contact potentials etc. were avoided. The accuracy of the energy scale is estimated as 1 eV. The onset for Kr ($^3P_1 \rightarrow {}^1S_0$) VUV fluorescence at 10.03 eV was also used for energy calibration [27]. (Note that here and elsewhere we use this simple L-S nomenclature for the $^3P_1$ state. More rigorously, because of the intermediate coupling situation it could be described as the $5s[3/2]_{J=1}$ state.)

3 Results and discussion

3.1 TOF data

Figure 1 shows the signal recorded at the detector as a function of time during and following the 1.6 μs electron pulse. Several time-of-flight (TOF) curves are shown (displaced upwards) at various electron energies for the clustered beam. The series of TOF curves taken at different electron-impact energies show the cluster fragmentation pattern and signal intensity varying significantly. Suitable biasing of the detector housing and of the channeltron itself excluded any scattered electrons or other charged particles. A prompt photon peak, coincident with the electron pulse, is the suppressed structure on the left of Figure 1. It exhibits a characteristic tail extending for many

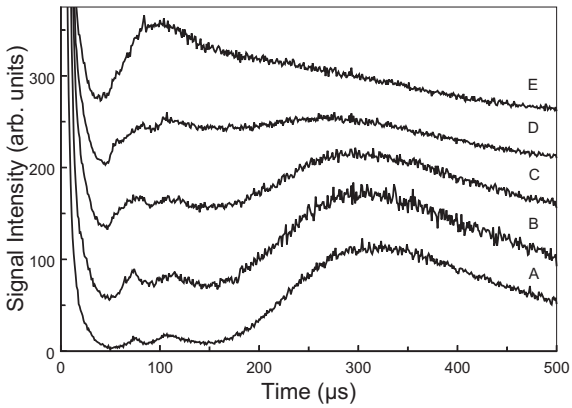

Fig. 1. Detector signal as a function of time. The incident electron beam energies are A: 20 eV; B: 30 eV; C: 40 eV; D: 50 eV; E: 100 eV. All time-of-flight curves are displaced upwards except for the 20 eV curve.

microseconds. This feature indicates that some of the excited Kr atoms or molecules are rather long lived. The TOF data demonstrate increasing signal intensity for the two peaks at intermediate flight times (referred to as the 75 μs and 112 μs peaks, respectively from the left) relative to the broad peak at longest flight times (referred to as the 320 μs peak). These peaks are due to the detection of metastable Kr atoms. At higher electron impact energies, the two peaks (75 μs and 112 μs) at intermediate flight times merge into a single peak. We note that because of its heavier mass and hence longer flight times, better resolution of these structures is achieved then was achieved for Ar [20].

Some of the structure observed at the longest flight times is due to randomly directed background krypton atoms which have been excited into metastable states as they pass through the electron beam. However, most of the structure is due to additional processes. The additional processes are evident from the observation that the maximum of the structure at the longest flight times (320 μs peak) shifts to shorter times with increasing electron beam energy. To illustrate the compound nature of this structure we follow the procedure outlined in reference [20]. We assume that the TOF distribution from a single process should be independent of incident electron energy and also that the TOF distribution taken at the lowest incident energy ($\sim$14 eV) should be representative of just a single process. Thus we take the shape of the feature peaked at 320 μs and scale it suitably so that it matches the trailing edge of the feature taken at 20 eV incident energy. This fit is represented by the solid curve in Figure 2. Subtraction of this scaled data from the original 20 eV data results in the data set shown in Figure 2. Deconvolution of these data into three separate structures is shown by the dotted lines in Figure 2. All of this reveals that at least four processes (numbered 1–4 in Fig. 2) are contributing to the observed spectrum. Excitation function observations (discussed later) will include further details on the indicated processes.

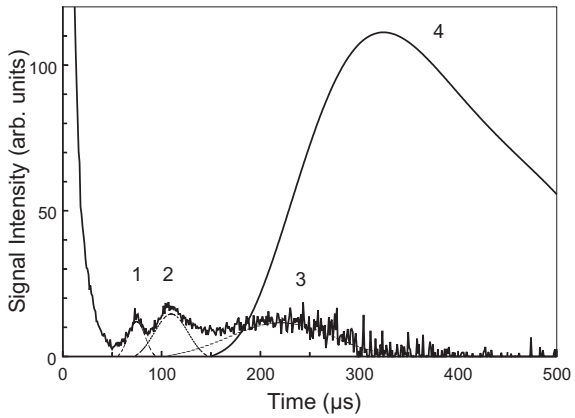

Fig. 2. Metastable signal, indicating at least four contributing processes, as a function of time after the electron beam pulse at 20 eV. The solid curve (4) with a maximum at 320 μs is representative of a process identified using lower incident electron energies (see text). Subtraction of this curve from the 20 eV data in Figure 1 yields the data set shown. The dotted curves represent an approximate deconvolution into three separate structures, 1–3.

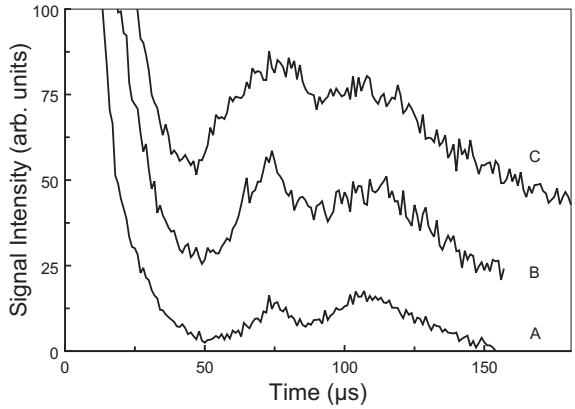

Fig. 3. Metastable signal due to processes 1 and 2 as a function of time after the electron beam pulse at incident energies of A: 20 eV, B: 30 eV, and C: 40 eV. The data have been retrieved from those of Figures 1 and 2 as discussed in the text. All curves are displaced upwards except for the 20 eV curve.

Removing processes 3 and 4 from the data of Figure 1 using a velocity distribution fit (see Ref. [28]), allows us to zero in on processes 1 and 2. The result is shown in Figure 3. Additional TOF data (not displayed) demonstrate that the two 75 μs and 112 μs peaks appear at approximately the same onset energy (within the energy resolution of our system). This is consistent with excitation function observations discussed later. The maxima of the two metastable peaks appear not to shift with increasing energy, though the first peak, which appears at the shortest flight times, is observed to broaden.

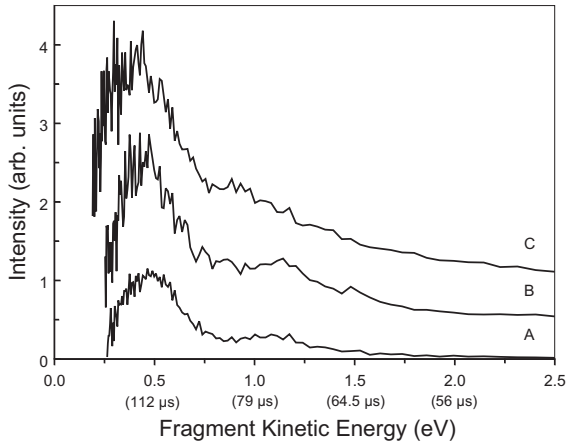

Fig. 4. Fragment kinetic energy spectra derived from the time-of-flight (TOF) data of Figure 3 (see text). Incident electron energies are A: 20 eV, B: 30 eV, and C: 40 eV. All curves are displaced upwards except for the 20 eV curve. Some TOF times are indicated in parentheses under their corresponding kinetic energies.

3.2 Kinetic energy analysis

The TOF data displayed in Figure 3 can be converted readily to fragment kinetic energy (FKE) data knowing the distance from the source to the detector, assuming that the mass of the detected fragment is known. See reference [29] for details. In this case, we assume that a krypton metastable atom is detected which originates from an excited dimer. This is reasonable based upon previous argon results [20].

Figure 4 presents fragment kinetic energy data at incident electron energies of 20, 30, and 40 eV obtained using the data of Figure 3. The main feature at all displayed electron energies is peaked at roughly 0.5 eV. This corresponds to the peak near 112 μs from the TOF data. As the incident electron energy increases, the maximum appears to shift slightly, from approximately 0.5 eV at 20 eV impact energy to approximately 0.4 eV at an impact energy of 40 eV. This 0.4 eV fragment kinetic energy value is fortuitously similar to the reported value of 0.4 eV obtained with solid targets using high energy (2.5 keV) electron impact [30]. The solid target observation was argued to be the result of the repulsion of ground-state atoms after radiative decay of vibrationally relaxed dimers (M band) [30]. The M band is recognized as the second continuum of the cluster fluorescence which results from strongly bound states, *i.e.*, $^{1,3}\Sigma_u^+$ [17].

The other metastable peak near 75 μs (in Fig. 3) gives rise to the FKE shoulder at an energy slightly greater than 1 eV. This is clearly a minor feature relative to the first FKE peak. As the incident electron energy increases, the shoulder around 1 eV becomes less prominent. The long tail to the FKE spectrum, which extends to higher values as the incident electron energy is increased, suggests that the inner repulsive wall of the parent-potential energy curve is being accessed or that new production channels are opening up. This is consistent with the slight

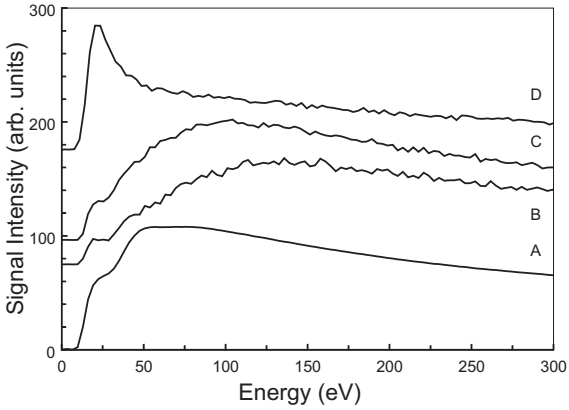

Fig. 5. Excitation functions appropriate to different time-of-flight windows (see Fig. 1): A: 0–5 μs, photons only; B: 50–90 μs; C: 90–150 μs; D: 150–850 μs. All curves, except A, are displaced upwards for clarity. See the text for further discussion.

broadening observed in the fastest metastable peak (near 75 μs), Figure 1. It should also be noted that the 215 μs metastable peak (process 3) corresponds to a fragment kinetic energy of about 0.14 eV. This peak was not transformed into a FKE curve because of poor signal-to-noise. This becomes particularly significant at longer times because of the t^3 factor that appears in the transformation (see Ref. [29]). We note that the 320 μs peak corresponds to a fragment kinetic energy of 0.06 eV, significantly higher than thermal.

3.3 Excitation functions

Figure 5 shows a series of excitation functions taken using different TOF windows as discussed in the experimental section. The curves are displaced upwards for clarity with additional details given in the caption. The windows are chosen to highlight the different features in Figure 1.

The bottom curve represents the excitation function of the prompt photons emitted coincident with or up to 5 μs after the exciting electron beam pulse. We note that the excitation function is broad with a maximum near 75 eV, indicating that the excitation process is optically allowed. The threshold is in the vicinity of 10 eV and a distinct shoulder is observed around 25 eV which indicates that a new excitation channel is opening. This additional photon-producing channel likely involves simultaneous excitation and ionization or possibly sequential excitation of two atoms in the cluster. The 10 eV onset is consistent with the threshold for exciting the atomic resonance lines, $^1\mathrm{P}_1 \rightarrow {}^1\mathrm{S}_0$ and $^3\mathrm{P}_1 \rightarrow {}^1\mathrm{S}_0$, within the energy resolution of our set-up. Lifetime measurements, not presented here, involving the trailing edge of the prompt photon peak, Figure 1, suggest that at least three different decays are contributing, one as long as 3.5 μs. Some of these will be due to decay of excimers within the cluster [15,18,19,32].

The second excitation function, for the time window 50–90 μs after the electron pulse, relates to process 1 and is seen (Fig. 5) to be broad with a maximum around 135 eV (with a local maximum near 20 eV), and a threshold at 11–12 eV referred to as process 1. Note that this excitation function has a TOF window that includes a portion of the other metastable signal from process 2 (peaked near 112 μs). An additional appearance energy was observed at about 27 eV, indicating the presence of an additional process which we will refer to as process 1a. This onset at approximately 27 eV likely corresponds to simultaneous excitation and ionization based upon similar argon results [20]. Process 1a yields fragments with kinetic energies of approximately 1 eV, similar to process 1 but with a relatively larger full width half maximum.

The third excitation function, for the time window 90–150 μs, is also broad with a maximum around 100 eV (with a local maximum near 20 eV), which demonstrates that different processes are dominant for this curve compared to the second excitation function. The mean kinetic energy of these fragments is around 0.5 eV (see Fig. 4) which is about half that of the fragments resulting from process 1. The process 2 threshold is observed near 11.5 eV with additional processes appearing at higher energies. As in the second excitation function, a second onset at approximately 27 eV was identified (process 2a), again with a fragment kinetic energy in the range of the FKE of process 2. The excitation functions have significant overlap with respect to the TOF peaks (see Figs. 1–3). The reason for the 27 eV onset of process 2a is probably similar to that for the sister excitation (process 1a) discussed above. Given the different excitation function shapes of processes 1a and 2a, and the different energies of the resulting fragments, different parent excited states must be involved.

The final (top) excitation function displayed in Figure 5, with a threshold near 10 eV, represents the excitation mainly of process 4. (This is shown as the broad peak at long flight times in Fig. 1.) Because these atoms are being detected hundreds of microseconds after the exciting electron pulse, they must be metastable in character, most likely the lowest lying metastable states, $5s[1/2]_{J=0}\ {}^3\mathrm{P}_0$ and $5s[3/2]_{J=2}\ {}^3\mathrm{P}_2$ states. The sharply peaked nature of the excitation function, with a maximum near 20 eV, indicates initial excitation *via* an exchange process to a state of different multiplicity to the ground state. Since krypton has a singlet ($^1\mathrm{S}_0$) ground state, the detected excited state must have a strong triplet contribution. It is well-known that the lowest lying excited metastable states of Kr have a strong triplet component [1,31,32]. Because the 320 μs peak dominates the signal in the lower energy region, an identification of the onset energy for the 215 μs peak (process 3) using excitation function data is not possible. However, TOF data suggest a threshold between 14 eV and 20 eV (certainly above 10 eV).

Figure 6 shows some potential energy curves for Kr_2 and indicates the known energy positions of the Kr atom and exciton energies. Data from references [8,13,16,27, 31,33–36] have been used to produce this figure. Excitation function and FKE observations along with Figure 6 indicate that the two fastest metastable fragments

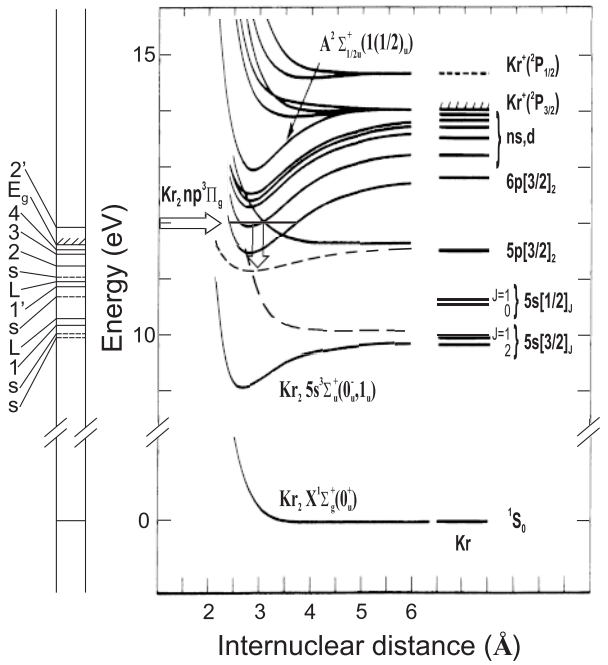

Fig. 6. (Left) Location of excitons in solid krypton [8,13,16,33,34]. Surface excitons are indicated by *s* (broken line) and solid lines are for bulk excitons (transverse and longitudinal). (Right) Schematic diagram of Kr_2 potential curves adapted from [31,35,36] with atom energy positions from [27, 35]. The arrows indicate a possible excitation scheme, such as that discussed in the text, for fast metastable atom production.

originate *via* a bound state of a manifold above the 5*s* states followed by decay to a repulsive state that leads to fragmentation. Interestingly, an infrared fluorescence experiment [37] on xenon dimers has recently demonstrated a broad continuum (centred at about 0.95 eV) that is likely produced by a bound-repulsive transition within the excited state manifold. A similar process may be occurring here. The 11–12 eV onsets of processes 1 and 2 (yielding the two fastest metastable fragments) suggest that these were likely produced *via* initial excitation of excitons in the cluster. Though our energy resolution does not allow for an exact exciton identification, it is known that Kr dimers undergo desorption from small Kr clusters (our clusters being somewhat larger, hundreds of atoms) only after excitation of surface states [14]. It should be noted that this Kr situation is different than the Ar case (see Refs. [14,20,21]) in that bulk excitons can cause Ar_2 desorption from cluster surfaces. An onset of 11 eV (with small Kr clusters) likely corresponds to the excitation of surface excitons close to this energy [8,13,16,33,34]. The approximately 27 eV threshold (processes 1a and 2a) is likely due to simultaneous ionization (14 eV) and excitation (around 13 eV), paralleling our previous Ar work [20]. The 10 eV threshold of the slowest fragments (process 4) indicates that here the excitation of the (small) cluster proceeds *via* a surface exciton near 10 eV, though an exact exciton identification can not be made within our energy resolution.

4 Conclusion

Time-of-flight and excitation function measurements of the fragmentation of neutral krypton clusters following electron impact have been presented. At least six different production mechanisms for metastable neutral fragments have been identified in addition to three different channels leading to prompt photon production.

The metastable neutral fragments were ejected from the cluster with energies in the range 0.06 to 1 eV. The particular energy distribution obtained depended on the excitation energy. The fragments with the highest kinetic energy resulted from the population and subsequent dissociation of repulsive states of Kr_2. Measured thresholds were in the neighbourhood of 10–12 eV suggesting that exciton production was occurring. Secondary thresholds at 27 eV likely involved simultaneous excitation and ionization or possibly two sequential excitations within the cluster.

The authors thank the staff of the mechanical and electronic workshops at the University of Windsor for expert technical help. The authors also are grateful to the Natural Sciences and Engineering Research Council of Canada (NSERC) for financial support. C.M. thanks NSERC for the award of a Postgraduate Scholarship.

References

1. M.F. Masters, J.E. Tucker, B.L. Wexler, S.K. Searles, J. Appl. Phys. **75**, 3777 (1994).
2. G. Gerasimov *et al.*, Appl. Phys. B **66**, 81 (1998).
3. G. Stark, P.L. Smith, in *Atomic, Molecular, & Optical Physics Handbook*, edited by G.W.F. Drake (AIP Press, Woodbury, New York, 1996), p. 490.
4. P.E. LaRocque, R.H. Lipson, P.R. Herman, B.P. Stoicheff, J. Chem. Phys. **84**, 6627 (1986).
5. G. Hilber, A. Lago, R. Wallenstein, J. Opt. Soc. Am. B **4**, 1753 (1987).
6. J.P. Marangos *et al.*, J. Opt. Soc. Am. B **7**, 1254 (1990).
7. J.W.G. Tisch *et al.*, J. Phys. B **30**, L709 (1997).
8. W. Kamke *et al.*, Z. Phys. D **14**, 339 (1989).
9. J. Krauss *et al.*, Z. Phys. D **20**, 29 (1991).
10. G. Ganteför, G. Bröker, E. Holub-Krappe, A. Ding, J. Chem. Phys. **91**, 7972 (1989).
11. R. Thissen *et al.*, Eur. Phys. J. D **4**, 335 (1998).
12. A. Knop, B. Wassermann, E. Rühl, Phys. Rev. Lett. **80**, 2302 (1998).
13. J. Stapelfeldt, J. Wörmer, T. Möller, Phys. Rev. Lett. **62**, 98 (1989).
14. T. Möller, Z. Phys. D **20**, 1 (1991).
15. E. Morikawa *et al.*, J. Chem. Phys. **91**, 1469 (1989).
16. T. Möller, G. Zimmerer, J. Opt. Soc. Am. B **6**, 1062 (1989).
17. R. Karnbach *et al.*, Chem. Phys. Lett. **203**, 248 (1993).
18. E.T. Verkhovtseva, E.A. Bondarenko, Yu.S. Doronin, Opt. Spectrosc. (USSR) **63**, 22 (1987); Chem. Phys. Lett. **140**, 181 (1988).
19. E.A. Bondarenko, E.T. Verkhovtseva, Yu.S. Doronin, A.M. Ratner, Chem. Phys. Lett. **182**, 637 (1991).

20. P.J.M. van der Burgt, J.W. McConkey, J. Chem. Phys. **102**, 8414 (1995).
21. W. Kedzierski, J.W. McConkey, J. Chem. Phys. **107**, 6521 (1997).
22. W. Kedzierski, M. Brennan, J.W. McConkey, Can. J. Phys. **76**, 985 (1998).
23. C. Malone, W. Kedzierski, J.W. McConkey, J. Phys. B **33**, 4863 (2000).
24. J. Wörmer, V. Guzielski, J. Stapelfeldt, T. Möller, Phys. Scripta **41**, 490 (1990); Chem. Phys. Lett. **159**, 321 (1989).
25. O.F. Hagena, Z. Phys. D **4**, 291 (1986).
26. T. Möller, J. Stapelfeldt, M. Beland, G. Zimmerer, Chem. Phys. Lett. **117**, 301 (1985).
27. C.E. Moore, *Atomic Energy Levels* (Circular of the National Bureau of Standards 467, 1952).
28. H. Haberland, U. Buck, M. Tolle, Rev. Sci. Instrum. **56**, 1712 (1985).
29. G. Allcock, J.W. McConkey, J. Phys. B **9**, 2127 (1976); L.R. LeClair, J.W. McConkey, J. Chem. Phys. **99**, 4566 (1993).
30. D.J. O'Shaughnessy, J.W. Boring, S. Cui, R.E. Johnson, Phys. Rev. Lett. **61**, 1635 (1988).
31. E. Audouard, F. Spiegelmann, J. Chem. Phys. **94**, 6102 (1991).
32. Y. Salaméro *et al.*, J. Phys. B **23**, 3569 (1990).
33. V. Saile, Appl. Opt. **19**, 4115 (1980).
34. M. Runne, G. Zimmerer, Nucl. Instr. Meth. Phys. Res. B **101**, 156 (1995).
35. D.B. Geohegan, J.G. Eden, J. Chem. Phys. **89**, 3410 (1988).
36. M. Hemici *et al.*, Phys. Rev. A **51**, 3351 (1995).
37. A.F. Borghesani, G. Bresi, G. Carugno, J. Chem. Phys. **115**, 6042 (2001).